

# The Fishyscapes Benchmark: Measuring Blind Spots in Semantic Segmentation

Hermann Blum\* Paul-Edouard Sarlin\* Juan Nieto Roland Siegwart Cesar Cadena  
Autonomous Systems Lab, ETH Zürich

## Abstract

Deep learning has enabled impressive progress in the accuracy of semantic segmentation. Yet, the ability to estimate uncertainty and detect failure is key for safety-critical applications like autonomous driving. Existing uncertainty estimates have mostly been evaluated on simple tasks, and it is unclear whether these methods generalize to more complex scenarios. We present *Fishyscapes*, the first public benchmark for uncertainty estimation in a real-world task of semantic segmentation for urban driving. It evaluates pixel-wise uncertainty estimates and covers the detection of both out-of-distribution objects and misclassifications. We adapt state-of-the-art methods to recent semantic segmentation models and compare approaches based on softmax confidence, Bayesian learning, and embedding density. A thorough evaluation of these methods reveals a clear gap to their alleged capabilities. Our results show that failure detection is far from solved even for ordinary situations, while our benchmark allows measuring advancements beyond the state-of-the-art.

## 1. Introduction

Deep learning has had a high impact on the precision of computer vision methods [1–4] and enabled semantic understanding in robotic applications [5–7]. However, while these algorithms are usually compared on closed-world datasets with a fixed set of classes [8, 9], the real-world is uncontrollable, and a wrong reaction by an autonomous agent to an unexpected input can have disastrous consequences [10].

As such, to reach full autonomy while ensuring safety and reliability, decision-making systems need information about outliers and uncertain or ambiguous cases that might affect the quality of the perception output. As illustrated in Figure 1, Deep CNNs react unpredictably for inputs that deviate from their training distribution. In the presence of an outlier object, this is interpolated with available classes, a behaviour similar to what is known in human perception as ‘blind spot’ [11]. Existing research to detect such behaviour is often labeled as out-of-distribution

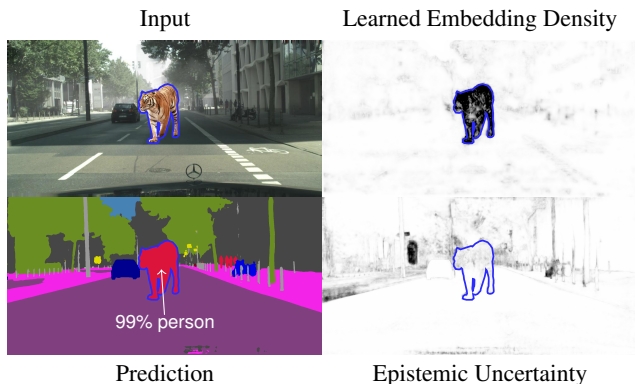


Figure 1. When exposed to an object type unseen during training (here a tiger), a state-of-the-art semantic segmentation model [1] predicts a familiar label (*person*) with high confidence. To detect such failures, we evaluate various methods that assign a pixel-wise out-of-distribution score, where higher values are darker. The blue outline is not part of the images and added for illustration.

(OoD), anomaly, or novelty detection, and has so far focused on developing methods for image classification, evaluated on simple datasets like MNIST or CIFAR-10 [12–20]. How these methods generalize to more elaborate network architectures and pixel-wise uncertainty estimation has not been assessed.

Motivated by these practical needs, we introduce *Fishyscapes*, a benchmark that evaluates uncertainty estimates for semantic segmentation. *Fishyscapes* is based on data from Cityscapes [9], a popular benchmark for classification accuracy in semantic segmentation, and consists of two parts: (i) *Fishyscapes* OoD overlays unknown objects on Cityscapes images. These objects need to be segmented, requiring an estimate of novelty or model uncertainty. (ii) *Fishyscapes* Misclassification assesses misclassification detection on conditions that are not part of the Cityscapes training data, such as fog, night, rain, and more geographically diverse scenes. To further test whether methods overfit on the set of OoD objects, we introduce a dynamic dataset that changes regularly and therefore enables the community to test for true novelty detection.

To provide a broad overview, we adapt a variety of methods to semantic segmentation that were originally designed for image classification, with examples listed in Figure 2.

\*authors contributed equally

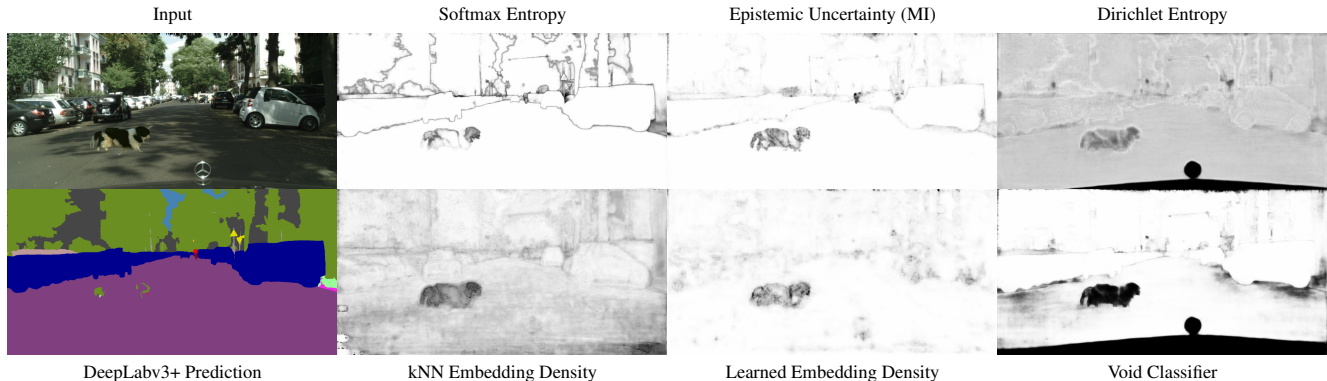


Figure 2. **Example of out-of-distribution (OoD) detection:** We evaluate the ability of Bayesian (top) and non-Bayesian (bottom) methods to segment OoD objects (here a dog) based on a semantic segmentation model. Better methods should assign a high score (dark) to pixels belonging to the object only, and a low score (white) to in-distribution (background) pixels. The semantic prediction is not sufficient.

Because segmentation networks are much more complex and have high computational costs, this adaptation is not trivial, and we suggest different approximations to overcome these challenges.

Our experiments show that the embeddings of intermediate layers hold important information for OoD detection. Based on recent work on generative models, we develop a novel method using density estimation in the embedding space. While the proposed approach outperforms all other methods for OoD detection, we stress that current uncertainty estimation and OoD detection do not achieve the accuracy required for safety-critical applications. We conclude that these remain open problems, with embedding density being an interesting path for further research.

To summarize, our contributions are the following:

- The first public benchmark evaluating pixel-wise uncertainty estimates in semantic segmentation, with a dynamic, self-updating dataset for OoD detection.
- We report an extensive evaluation with diverse state-of-the-art approaches to uncertainty estimation, adapted to the semantic segmentation task, and present a novel method for OoD detection.
- We show a clear gap between the alleged capabilities of established methods and their performance on this real-world task, thereby confirming the necessity of our benchmark to support further research in this direction.

## 2. Related Work

Here we review the most relevant works in semantic segmentation and their benchmarks, and methods that aim at providing a confidence estimate of the output of deep networks.

### 2.1. Semantic Segmentation

**State-of-the-art models** are fully-convolutional deep networks trained with pixel-wise supervision. Most works [1, 21–23] adopt an encoder-decoder architecture that initially reduces the spatial resolution of the feature maps, and subsequently upsamples them with learned transposed convolution, fixed bilinear interpolation, or unpooling. Additionally, dilated convolutions or spatial pyramid pooling enlarge the receptive field and improve the accuracy.

**Popular benchmarks** compare methods on the segmentation of objects [24] and urban scenes. In the latter case, Cityscapes [9] is a well-established dataset depicting street scenes in European cities with dense annotations for a limited set of classes. Efforts have been made to provide datasets with increased diversity, either in terms of environments, with WildDash [25], which incorporates data from numerous parts of the world, or with Mapillary [26], which adds many more classes. Like ours, some datasets are explicitly derived from Cityscapes, the most relevant being Foggy Cityscapes [27], which overlays synthetic fog onto the original dataset to evaluate more difficult driving conditions. The Robust Vision Challenge<sup>1</sup> also assesses generalization of learned models across different datasets.

**Robustness and reliability** are only evaluated by all these benchmarks through ranking methods according to their accuracy, without taking into account the uncertainty of their predictions. Additionally, despite one cannot assume that models trained with closed-world data will only encounter known classes, these scenarios are rarely quantitatively evaluated. To our knowledge, WildDash [25] is the only benchmark that explicitly reports uncertainty w.r.t. OoD examples. These are however drawn from a very limited set of full-image outliers, while we introduce a diverse set of objects, as WildDash mainly focuses on accuracy.

<sup>1</sup><http://www.robustvision.net/>

Bevandic *et al.* [28] experiment with OoD objects for semantic segmentation by overlaying objects on Cityscapes images in a manner similar to ours. They however assume the availability of a large OoD dataset, which is not realistic in an open-world context, and thus mostly evaluate supervised methods. In contrast, we assess a wide range of methods that do not require OoD data. Mukhoti & Gal [29] introduce a new metric for uncertainty evaluation and are the first to quantitatively assess misclassification for segmentation. Yet they only compare few methods on normal in-distribution (ID) data.

## 2.2. Uncertainty estimation

There is a large body of work that aims at detecting OoD data or misclassification by defining uncertainty or confidence estimates.

**The softmax score**, *i.e.* the classification probability of the predicted class, was shown to be a first baseline [14], although sensitive to adversarial examples [30]. Its performance was improved by ODIN [31], which applies noise to the input with the Fast Gradient Sign Method (FGSM) [30] and calibrates the score with temperature scaling [32].

**Bayesian deep learning** [33, 34] adopts a probabilistic view by designing deep models whose outputs and weights are probability distributions instead of point estimates. Uncertainties are then defined as dispersions of such distributions, and can be of several types. *Epistemic* uncertainty, or model uncertainty, corresponds to the uncertainty over the model parameters that best fit the training data for a given model architecture. As evaluating the posterior over the weights is intractable in deep non-linear networks, recent works perform Monte-Carlo (MC) sampling with dropout [35] or ensembles [36]. *Aleatoric* uncertainty, or data uncertainty, arises from the noise in the input data, such as sensor noise. Both have been applied to semantic segmentation [34], and successively evaluated for misclassification detection [29], but only in controlled and ideal conditions, and without comparing to non-Bayesian approaches. Malinin & Gales [12] later suggested that *epistemic* and *aleatoric* uncertainties are only meaningful for inputs that match the training distribution, and that a third kind, *distributional* uncertainty, is required to represent model misspecification with respect to OoD inputs. Their approach however was only applied to image classifications on toy datasets, and requires OoD data during the training stage. To address the latter constraint, Lee *et al.* [37] earlier proposed a Generative Adversarial Network (GAN) that generates OoD data as boundary samples. This is however not possible for complex and high-dimensional data like high-resolution images of urban scenes.

**OoD and novelty detection** is often tackled by non-Bayesian approaches, which explicitly do not require ex-

amples of OoD data at training time. As such, feature introspection amounts to measuring discrepancies between distributions of deep features of training data and OoD samples, using either nearest neighbour (NN) statistics [13, 38] or Gaussian approximations [15]. These methods have the benefit of working on any classification model without requiring specific training. On the other hand, approaches specifically tailored to perform OoD detection include one-class classification [16, 17], which aim at creating discriminative embeddings, density estimation [18, 39], which estimate the likelihood of samples w.r.t to the true data distribution, and generative reconstruction [19, 20], which use the quality of auto-encoder reconstructions to discriminate OoD samples. Richter *et al.* [40] apply the latter to simple real images recorded by a robotic car and successfully detect new environments. Yet all of these methods are only applied to image classification models for OoD detection on toy datasets or for adversarial defense. As such, it is not trivial to adapt these methods to the more complex architectures used in semantic segmentation, and to the scale required by large input images.

## 3. Benchmark Design

In the following we describe our *Fishyscapes* benchmark: (i) the overall motivations and philosophy; (ii) the datasets and their creation; and (iii) the metrics used for comparisons in the OoD and misclassification tasks.

### 3.1. Philosophy

Because it is not possible to produce ground truth for uncertainty values, evaluating estimators is not a straightforward task. We thus compare them on the two proxy classification tasks [14] of detecting OoD inputs and discriminating correct and wrong predictions of a semantic segmenter. The uncertainty estimates are seen as scores of a binary classifier that compares the score against a threshold and whose performance reflects the suitability of the estimated uncertainty for the respective tasks. Such an approach however introduces a major issue for the design of a public OoD detection benchmark. With a publicly available ID training dataset  $A$  and OoD inputs  $B$ , it is not possible to distinguish between an uncertainty method that informs a classifier to discriminate  $A$  from any other input, and a classifier trained to discriminate  $A$  from  $B$ . The latter option clearly does not represent progress towards the goal of general uncertainty estimation, but rather overfitting.

To this end, we (i) only release a small validation set with associated ground truth OoD masks, while keeping larger test sets hidden, and (ii) continuously evaluate submitted methods against a dynamically changing dataset. This setup preserves the uncertainty as to which OoD objects might be encountered in the real world. To encourage unsupervised methods, we stress that the validation set is for

parameter tuning only, and should not be used to train models. The evaluation is performed remotely using executables submitted by the participants.

Our Fishyscapes benchmark is composed of two test sets for OoD and one for misclassification detection. The OoD datasets are composed of in-distribution background images of urban scenes originated from the same data distribution used to train the semantic segmentation model. On top of those are overlaid unknown objects, like animals, never seen during the training of the model. One test set, *FS OoD*, is fixed, while the other, *FS OoD Dynamic* is automatically updated every few months.

Using their executables, methods submitted to the benchmark are continuously evaluated on every new version of the dynamic dataset. This enables us to evaluate methods on data that was not existent at the time of submission to the benchmark, assessing their generalization capabilities. Independent from their submission time, methods can always be compared using the fixed test set.

### 3.2. Datasets

**FS OoD** is based on the validation set of Cityscapes [9]. It has a limited visual diversity, which is important to make sure that it contains none of the overlaid OoD objects. In addition, background pixels originally belonging to the void class are excluded from the evaluation, as they may be borderline OoD. Artificial OoD examples are extracted from the generic Pascal VOC [24] dataset using the associated segmentation masks. We only overlay objects from classes that cannot be found in Cityscapes: *aeroplane, bird, boat, bottle, cat, chair, cow, dog, horse, sheep, sofa, tvmonitor*. Objects cropped by the image borders or objects that are too small to be seen are filtered out. We randomly size and position the objects on the underlying image, making sure that none of the objects appear on the ego-vehicle. Objects from mammal classes have a higher probability of appearing on the lower-half of the screen, while classes like birds or airplanes have a higher probability for the upper half. The placing is not further limited to ensure each pixel in the image, apart from the ego-vehicle, is comparably likely to be OoD. To make the task of outlier detection harder, we modify the color tone and brightness of the overlays according to the pixels below the objects, while we add synthetic fog [41, 42] on the in-distribution pixels with a per-image probability. This prevents fraudulent methods to compare the input against a fixed set of Cityscapes images. The dataset is split into a minimal public validation set of 30 images and a hidden test set of 1000 images. It contains in total around 4.5e7 OoD and 1.8e9 ID pixels. The validation set only contains a small disjoint set of pascal objects to prevent few-shot learning on our data creation method.

**FS OoD Dynamic** is built similarly to FS OoD, but with

overlay objects crawled from the internet using a list of keywords. Our script searches for images with transparent background, uploaded in a recent timeframe, and filters out images that are too small. The only manual process is filtering out images that are not suitable, *e.g.* with decorative borders. The dataset for March 2019 contains 4.9e7 OoD and 1.8e9 ID pixels and is not publicly released.

**Misclassification** is measured on a mix of four different datasets. Foggy Driving [41] and Foggy Zurich [42] are small datasets with real images of foggy driving conditions. We filter out all images where the occlusion by fog is too strong and make sure any non-classifiable objects are labelled with the void class. WildDash [25] is a collection of very diverse dash cam images labelled with the same set of classes as Cityscapes. We combine all these datasets together with a random sample of 50 images from Mapillary vistas [26], downsampled to have similar sizes. In total, the 185 images form a balanced mixture of different conditions with hard-to-classify, ID examples.

### 3.3. Metrics

**OoD Detection.** We consider metrics associated with a binary classification task. Since the ID and OoD data is unbalanced, metrics based on the receiver operating curve (ROC) are not suitable. We therefore base the ranking and primary evaluation on the average precision (AP). However, as the number of false positives in high-recall areas is also relevant for safety-critical applications, we additionally report the false positive rate (FPR) at 95% true positive rate (TPR). This metric was also used in [14] and emphasizes safety.

**Misclassification.** High uncertainty for a pixel should indicate that the classification is not confident. However, the output class in a case of high uncertainty may still match the ground truth by chance. A metric simply measuring the detection performance is therefore not measuring the performance of uncertainty estimation correctly. Mukhoti & Gal [29] introduce PAVPU to address this problem:

$$\text{PAvPU} = \frac{n_{\text{accurate and certain}} + n_{\text{inaccurate and uncertain}}}{n_{\text{total}}} \quad (1)$$

Unfortunately, PAVPU and its maximum value depend on the accuracy of the semantic segmentation and therefore cannot be used to compare different models. However, the same objective can also be measured using Youden’s J (J) statistic [43], which is defined for our problem as:

$$J = \frac{n_{\text{accurate and certain}}}{n_{\text{accurate}}} + \frac{n_{\text{inaccurate and uncertain}}}{n_{\text{inaccurate}}} - 1 \quad (2)$$

Normalizing by the number of accurate and inaccurate predictions, this metric is independent from the actual classification accuracy of the semantic segmentation. Dealing

with pixel-wise uncertainty, the decision about certain or uncertain is done for every pixel comparing against a variable threshold. We then report the maximum J, which is the maximum possible probability of an informed decision, compared to a random one, given the information in the estimated uncertainty. Additionally, while not exactly capturing the performance of uncertainty estimation, we report the AP of misclassification detection for applications where this detection is prioritized over uncertainty estimation.

**Semantic Classification** is not the goal of our benchmark, but uncertainty estimation and outlier detection should not come at high cost of performance. We therefore report the mean intersection over union (IoU) of the segmentations.

## 4. Evaluated Methods

We now present the methods that are evaluated in Fishyscapes. In a first part, we describe the existing baselines and how we adapted them to the task of semantic segmentation. A novel method based on learned embedding density is then presented. Full experimental details are provided in appendix B. All approaches are applied to the state-of-the-art semantic segmentation model DeepLab-v3+ [1]. Here we do not always distinguish OoD and misclassification as some methods might be applicable to both.

### 4.1. Baselines

**Softmax score.** The maximum softmax probability is a commonly used baseline and was evaluated in [14] for OoD detection. We apply the metric pixel-wise and additionally measure the softmax entropy, as proposed by [37], which captures more information from the softmax.

**Training with OoD.** While we generally strive for methods that are not biased by data, learning confidence from data is an obvious baseline and was explored in [44]. As we are not supposed to know the true known distribution, we do not use Pascal VOC, but rather approximate unknown pixels with the Cityscapes void class. In our evaluation, we (i) train a model to maximise the softmax entropy for OoD pixels, or (ii) introduce void as an additional output class and train with it. The uncertainty is then measured as (i) the softmax entropy, or (ii) the score of the void class.

**Bayesian DeepLab** was introduced by Mukhoti & Gal [29], following Kendall & Gal [34], and is the only uncertainty estimate already applied to semantic segmentation in the literature. The epistemic uncertainty is modeled by adding Dropout layers to the encoder, and approximated by  $T$  MC samples, while the aleatoric uncertainty corresponds to the spread of the categorical distribution. The total uncertainty is the predictive entropy of the distribution  $\mathbf{y}$ ,

$$\hat{\mathbb{H}}[\mathbf{y}|\mathbf{x}] = - \sum_c \left( \frac{1}{T} \sum_t y_c^t \right) \log \left( \frac{1}{T} \sum_t y_c^t \right), \quad (3)$$

where  $y_c^t$  is the probability of class  $c$  for sample  $t$ . The epistemic uncertainty is measured as the mutual information (MI) between  $\mathbf{y}$  and the weights  $\mathbf{w}$ ,

$$\hat{\mathbb{I}}[\mathbf{y}, \mathbf{w}|\mathbf{x}] = \hat{\mathbb{H}}[\mathbf{y}|\mathbf{x}] - \frac{1}{T} \sum_{c,t} y_c^t \log y_c^t. \quad (4)$$

**Dirichlet Prior Networks** [12] extend the framework of [33] by considering the predicted logits  $\mathbf{z}$  as log concentration parameters  $\boldsymbol{\alpha}$  of a Dirichlet distribution, which is a prior of the predictive categorical distribution  $\mathbf{y}$ . Intuitively, the spread of the Dirichlet prior should model the distributional uncertainty, and remain separate from the data uncertainty modelled by the spread of the categorical distribution. To this end, Malinin & Gales [12] advocate to train the network with the objective:

$$\begin{aligned} \mathcal{L}(\theta) = & \mathbb{E}_{p_{\text{in}}} [\text{KL}[\text{Dir}(\boldsymbol{\mu}|\boldsymbol{\alpha}_{\text{in}}) || p(\boldsymbol{\mu}|\mathbf{x}; \boldsymbol{\theta})]] \\ & + \mathbb{E}_{p_{\text{out}}} [\text{KL}[\text{Dir}(\boldsymbol{\mu}|\boldsymbol{\alpha}_{\text{out}}) || p(\boldsymbol{\mu}|\mathbf{x}; \boldsymbol{\theta})]] \\ & + \text{CrossEntropy}(\mathbf{y}, \mathbf{z}). \end{aligned} \quad (5)$$

The first term forces ID samples to produce sharp priors with a high concentration  $\boldsymbol{\alpha}_{\text{in}}$ , computed as the product of smoothed labels and a fixed scale  $\alpha_0$ . The second term forces OoD samples to produce a flat prior with  $\boldsymbol{\alpha}_{\text{out}} = \mathbf{1}$ , effectively maximizing the Dirichlet entropy, while the last one helps the convergence of the predictive distribution to the ground truth. We model pixel-wise Dirichlet distributions, approximate OoD samples with void pixels, and measure the Dirichlet differential entropy.

**kNN Embedding.** Different works [13, 38] estimate uncertainty using kNN statistics between inferred embedding vectors and their neighbors in the training set. They then compare the classes of the neighbors to the prediction, where discrepancies indicate uncertainty. In more details, a given trained encoder maps a test image  $\mathbf{x}'$  to an embedding  $\mathbf{z}'_l = \mathbf{f}_l(\mathbf{x}')$  at layer  $l$ , and the training set  $\mathbf{X}$  to a set of neighbors  $\mathbf{Z}_l := \mathbf{f}_l(\mathbf{X})$ . Intuitively, if  $\mathbf{x}'$  is OoD, then  $\mathbf{z}'$  is also differently distributed and has *e.g.* neighbors with different classes. Adapting these methods to semantic segmentation faces two issues: (i) The embedding of an intermediate layer of DeepLab is actually a map of embeddings, resulting in more than 10,000 kNN queries for each layer, which is computationally infeasible. We follow [38] and pick only one layer, selected using the validation set. (ii) The embedding map has a lower resolution than the input and a given training embedding  $\mathbf{z}_l^{(i)}$  is therefore not associated with one, but with multiple output labels. As a baseline approximation, we link  $\mathbf{z}'_l$  to all classes in the associated image patch. The relative density [38] is then:

$$D(\mathbf{z}') = \frac{\sum_{i \in K, c' = c_i} \exp\left(-\frac{\mathbf{z}' \cdot \mathbf{z}_l^{(i)}}{|\mathbf{z}'| |\mathbf{z}_l^{(i)}|}\right)}{\sum_{i \in K} \exp\left(-\frac{\mathbf{z}' \cdot \mathbf{z}_l^{(i)}}{|\mathbf{z}'| |\mathbf{z}_l^{(i)}|}\right)}. \quad (6)$$

Here,  $c_i$  is the class of  $\mathbf{z}^{(i)}$  and  $c'$  is the class of  $\mathbf{z}'$  in the downsampled prediction. In contrast to [38], we found that the cosine similarity from [13] works well without additional losses. Finally, we upsample the density of the feature map to the input size, assigning each pixel a density value.

As the class association is unclear for encoder-decoder architectures, we also evaluate the density estimation with  $k$  neighbors independent of the class:

$$D(\mathbf{z}') = \sum_{i \in K} \exp\left(-\frac{\mathbf{z}' \cdot \mathbf{z}^{(i)}}{|\mathbf{z}'| |\mathbf{z}^{(i)}|}\right). \quad (7)$$

This assumes that an OoD sample  $\mathbf{x}'$ , with a low density w.r.t  $\mathbf{X}$ , should translate into  $\mathbf{z}'$  with a low density w.r.t.  $\mathbf{Z}_l$ .

## 4.2. Learned Embedding Density

We now introduce a novel approach that takes inspiration from density estimation methods while greatly improving their scalability and flexibility.

**Density estimation** using kNN has two weaknesses. First, the estimation is a very coarse isotropic approximation, while the distribution in feature space might be significantly more complex. Second, it requires to store the embeddings of the entire training set and to run a large number of NN searches, both of which are costly, especially for large input images. On the other hand, recent works [18, 39] on OoD detection leverage more complex generative models, such as normalizing flows [45–47], to directly estimate the density of the input sample  $\mathbf{x}$ . This is however not directly applicable to our problem, as (i) learning generative models that can capture the entire complexity of *e.g.* urban scenes is still an open problem; and (ii) the pixel-wise density required here should be conditioned on a very (ideally infinitely) large context, which is computationally intractable.

**Our approach** mitigates these issues by learning the density of  $\mathbf{z}$ . We start with a training set  $\mathbf{X}$  drawn from the unknown true distribution  $\mathbf{x} \sim p^*(\mathbf{x})$ , and corresponding embeddings  $\mathbf{Z}_l$ . A normalizing flow with parameters  $\theta$  is trained to approximate  $p^*(\mathbf{z}_l)$  by minimizing the negative loglikelihood (NLL) over all training embeddings in  $\mathbf{Z}_l$ :

$$\mathcal{L}(\mathbf{Z}_l) = -\frac{1}{|\mathbf{Z}_l|} \sum_i \log p_{\theta}(\mathbf{z}_l^{(i)}). \quad (8)$$

The flow is composed of a bijective function  $\mathbf{g}_{\theta}$  that maps an embedding  $\mathbf{z}_l$  to a latent vector  $\eta$  of identical dimensionality and with Gaussian prior  $p(\eta) = \mathcal{N}(\eta; 0, \mathbf{I})$ . Its loglikelihood is then expressed as

$$\log p_{\theta}(\mathbf{z}_l) = \log p(\eta) + \log \left| \det \left( \frac{d\mathbf{g}_{\theta}}{d\mathbf{z}} \right) \right|, \quad (9)$$

and can be efficiently evaluated for some constrained  $\mathbf{g}_{\theta}$ . At test time, we compute the embedding map of an input image, and estimate the NLL of each of its embeddings. In our

experiments, we use the Real-NVP bijector [45], composed of a succession of affine coupling layers, batch normalizations, and random permutations.

The benefits of this method are the following: (i) A normalizing flow can learn more complex distributions than the simple kNN kernel or mixture of Gaussians used by [15], where each embedding requires a class label, which is not available here; (ii) Features follow a simpler distribution than the input images, and can thus be correctly fit with simpler flows and shorter training times; (iii) The only hyperparameters are related to the architecture and the training of the flow, and can be cross-validated with the NLL of ID data without any OoD data; (iv) The training embeddings are efficiently summarized in the weights of the generative model with a very low memory footprint.

**Input preprocessing** [31] can be trivially applied to our approach. Since the NLL estimator is an end-to-end network, we can compute the gradients of the average NLL w.r.t. the input image by backpropagating through the flow and the encoder. In appendix B.6, we note consistent performance gains and tune the noise parameter on the validation set.

**A flow ensemble** can be built by training separate density estimators over different layers of the segmentation model, similar to [15]. However, the resulting NLL estimates cannot be directly aggregated as is, because the different embedding distributions have varying dispersions and dimensions, and thus densities with very different scales. We propose to normalize the NLL  $N(\mathbf{z}_l)$  of a given embedding by the average NLL of the training features for that layer:

$$\bar{N}(\mathbf{z}_l) = N(\mathbf{z}_l) - \mathcal{L}(\mathbf{Z}_l). \quad (10)$$

This is in fact a MC approximation of the differential entropy of the flow, which is intractable. In the ideal case of a multivariate Gaussian,  $\bar{N}$  corresponds to the Mahalanobis distance used by [15]. We can then aggregate the normalized, resized scores over different layers. We experiment with two strategies: (i) Using the minimum detects a pixel as OoD only if it has low likelihood through all layers, thus accounting for areas in the feature space that are in-distribution but contain only few training points; (ii) Following [15], taking a weighted average, with weights given by a logistic regression fit on a small validation set containing OoD, captures the interaction between the layers.

## 5. Discussion of Results

We show in Table 1 and Figure 3 the results of our benchmark for the aforementioned datasets and methods. Qualitative examples of the best performing methods are shown in figures 4 and 5.

**OoD Detection.** Confirming findings on simpler tasks [15], the softmax confidence does not provide the best results

| method                                  | score                  | FS OoD        |                                     | FS OoD-Dynamic |                                     | FS Misclassification |               |      | requires retraining | requires OoD data | Cityscapes mIoU |
|---|------------------------|---------------|-------------------------------------|----------------|-------------------------------------|----------------------|---------------|------|---------------------|-------------------|-----------------|
|   |                        | AP $\uparrow$ | FPR <sub>95%</sub> TPR $\downarrow$ | AP $\uparrow$  | FPR <sub>95%</sub> TPR $\downarrow$ | max J $\uparrow$     | AP $\uparrow$ | mIoU |                     |                   |                 |
| Baseline                                | random uncertainty     | 02.5          | 95.0                                | 02.6           | 95.0                                | 00.0                 | 38.9          | 45.5 | ✗                   | ✗                 | 80.3            |
| Softmax                                 | max-probability        | 12.9          | 39.8                                | 17.7           | 33.6                                | 43.6                 | 67.4          | 45.5 | ✗                   | ✗                 | 80.3            |
|   | entropy                | 15.4          | 39.8                                | 23.6           | 33.4                                | 43.5                 | 68.4          |      |                     |                   |                 |
| OoD training                            | max-entropy            | 27.5          | 23.6                                | 33.8           | 21.8                                | <b>44.3</b>          | 71.3          | 35.8 | ✓                   | ✓                 | 79.0            |
|   | void classifier        | 45.0          | 19.4                                | 52.9           | 13.3                                | (70.0)               | (93.4)        | 32.3 |                     |                   | 70.4            |
| Bayesian DeepLab                        | mutual information     | 48.7          | 15.5                                | 52.1           | 15.9                                | 40.7                 | 70.4          | 30.3 | ✓                   | ✗                 | 73.8            |
|   | predictive entropy     | 38.7          | 21.5                                | 40.1           | 21.5                                | 41.6                 | <b>73.8</b>   |      |                     |                   |                 |
| Dirichlet DeepLab                       | prior entropy          | 31.3          | 84.6                                | 27.7           | 93.6                                | 29.7                 | 65.0          | 37.5 | ✓                   | ✓                 | 70.5            |
| kNN Embedding                           | density                | 49.7          | 21.6                                | 48.0           | 17.4                                | 40.7                 | 68.0          | 45.5 | ✗                   | ✗                 | 80.3            |
|   | relative class density | 15.8          | -                                   | 20.4           | -                                   | 31.7                 | 58.0          |      |                     |                   |                 |
| <b>Learned Embedding Density (ours)</b> | single-layer NLL       | 55.4          | 24.0                                | 72.1           | 13.9                                | -                    | -             |      | ✗                   | ✗                 |                 |
|   | logistic regression    | 61.5          | <b>10.4</b>                         | 75.3           | <b>4.7</b>                          | -                    | -             | -    | ✗                   | ✓                 | 80.3            |
|   | minimum NLL            | <b>64.6</b>   | 22.4                                | <b>80.3</b>    | 12.7                                | -                    | -             |      |                     | ✗                 |                 |

Table 1. **Benchmark Results.** The gray columns mark the primary metrics of each benchmark dataset. We do not evaluate the learned embedding density on FS Misclassification as it is not designed for this task.

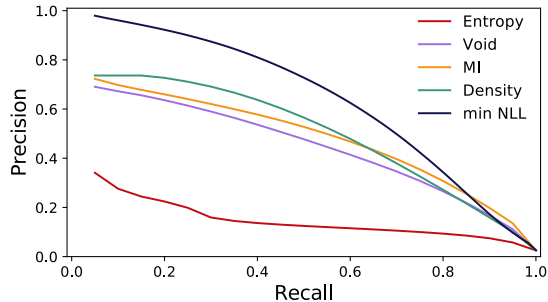


Figure 3. **Precision-Recall curve** for the best performing methods of each kind on the FS OoD dataset.

for OoD detection. While training with OoD data clearly improves the softmax-based detection, it is not better than other methods that do not require such data. One of these is Bayesian Deeplab, for which we find that the mutual information detects OoD better than the predictive entropy, which is in line with [34]. Its relatively low performance in the benchmark however shows that the estimated epistemic uncertainty does not correlate very well with the observation of OoD data. This supports the idea of an additional distributional uncertainty [12]. Yet, Dirichlet DeepLab, which attempts to model such uncertainty, gives poor results due to the unstable optimization of the KL divergence. Finally, embedding density based methods show an alternative route with outstanding results on our benchmark. We find that looking at more than one layer is beneficial, while different strategies improve either the general detection performance or the safety-critical FPR<sub>95%</sub> TPR.

Most of the results on the fixed dataset are reflected in the dynamic one. While the dynamic dataset is in general easier, due to the diversity of the OoD objects, the learned embedding density remains superior. The kNN based methods do not follow the same trend. We explain this by the higher modelling flexibility of the learned density, and its absence of hyperparameter tuning, preventing any overfitting on the validation set.

**Misclassification** Differently from OoD detection, the softmax score is expected to be a good indicator for classification uncertainty, and indeed shows competitive results. We note that the results for the void classifier are meaningless since a high void output score produces the exact misclassification it is detecting. For Bayesian DeepLab, we find the predictive entropy to be a better indicator of misclassification, which was also observed by [34]. The kNN density shows results similar to the other methods, hinting that embedding-based methods cannot be entirely classified as OoD-specific, but may also be able to detect input noise that is very different from the training distribution. Overall, the benchmark does not reveal a single method that performs significantly better than others.

**Challenges in Method Adaptation.** The results reveal that some methods cannot be easily adapted to semantic segmentation. For example, retraining required by special losses can impair the segmentation performance, which can be an issue for certain applications. As such, training Dirichlet DeepLab with a KL divergence can be particularly unstable, resulting in poor performance. This shows the advantage of methods that do not require retraining, such as our learned embedding density. Additionally, the benchmark shows uncompetitive results for class-based embedding, which only highlights the ambiguity of class association between features and predictions.

## 6. Conclusion

In this work, we introduced *Fishyscapes*, a benchmark for novelty detection and uncertainty estimation in the real-world setting of semantic segmentation for urban driving. Comparing state-of-the-art methods on this complex task for the first time, we draw multiple conclusions:

- Progress in uncertainty estimation for data like MNIST does not directly translate to real-world tasks. This holds

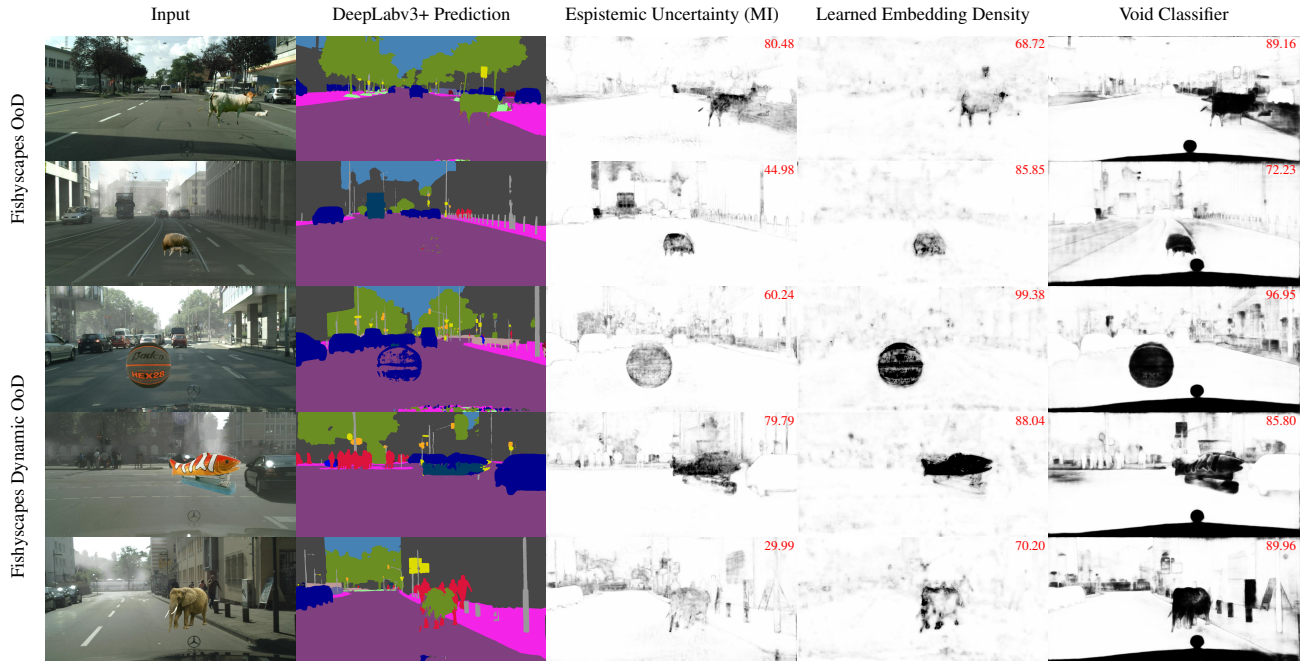


Figure 4. **Qualitative examples of OoD detection** in Fishyscapes OoD (rows 1-2) and Fishyscapes OoD Dynamic (rows 3-5). Better methods should assign a high score (dark) to the overlaid object. None of the methods perfectly detects all objects. The void classifier tends to assign high scores to some localized in-distribution areas. We report the AP of each score map in its top right corner.

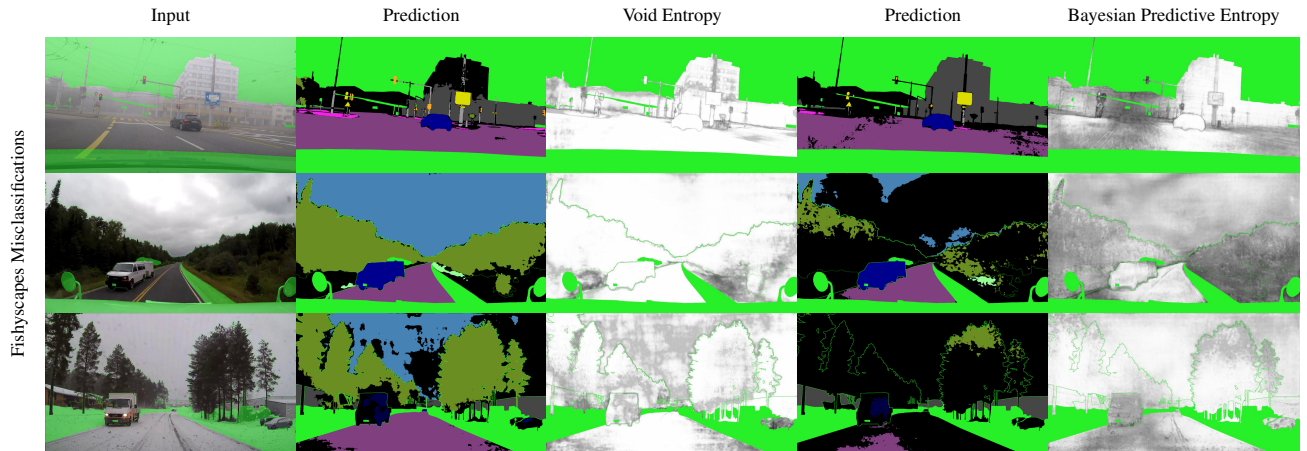


Figure 5. **Qualitative examples of misclassification detection.** Predictions correspond to the uncertainty maps to their right. Misclassifications are marked in black, while ignored *void* pixels are marked in bright green. Better methods should assign a high score (dark) to misclassified pixels. While the different trainings clearly lead to different classification performances, none of the methods captures all the misclassified pixels.

especially for the introduction of additional losses, which are harder to balance with more complex architectures.

- Learning uncertainty estimation from OoD data does not give better results than using methods that do not require such data, at least when the training data is far from the OoD test data.
- The proposed Learned Embedding Density is a promising direction of research as it outperforms all existing methods and can be applied to any of-the-shelf network

without requiring extensive hyperparameter tuning.

- The softmax output is a surprisingly competitive baseline for misclassification detection, albeit far from perfect.

Overall, despite the apparent progress, both OoD and misclassification detections are unsolved tasks. To deploy semantic segmentation methods in safety-critical and autonomous systems, further research is required. As a public benchmark, *Fishyscapes* supports the evaluation of new methods on such realistic scenarios.

## References

- [1] L.-C. Chen, Y. Zhu, G. Papandreou, F. Schroff, and H. Adam, "Encoder-decoder with atrous separable convolution for semantic image segmentation," in *ECCV*, 2018. DOI: [10.1007/978-3-030-01234-2\\_49](https://doi.org/10.1007/978-3-030-01234-2_49).
- [2] K. He, G. Gkioxari, P. Dollar, and R. Girshick, "Mask R-CNN," in *ICCV*, 2017. DOI: [10.1109/ICCV.2017.322](https://doi.org/10.1109/ICCV.2017.322).
- [3] H. Fu, M. Gong, C. Wang, K. Batmanghelich, and D. Tao, "Deep ordinal regression network for monocular depth estimation," in *CVPR*, 2018. DOI: [10.1109/CVPR.2018.00214](https://doi.org/10.1109/CVPR.2018.00214).
- [4] D. Sun, X. Yang, M. Liu, and J. Kautz, "PWC-Net: CNNs for optical flow using pyramid, warping, and cost volume," in *CVPR*, 2018. DOI: [10.1109/CVPR.2018.00931](https://doi.org/10.1109/CVPR.2018.00931).
- [5] J. McCormac, R. Clark, M. Bloesch, A. Davison, and S. Leutenegger, "Fusion++: Volumetric Object-Level SLAM," in *International Conference on 3D Vision (3DV)*, 2018. DOI: [10.1109/3DV.2018.00015](https://doi.org/10.1109/3DV.2018.00015).
- [6] P. R. Florence, L. Manuelli, and R. Tedrake, "Dense object nets: Learning dense visual object descriptors by and for robotic manipulation," in *Conference on Robot Learning (CoRL)*, 2018.
- [7] M. Liang, B. Yang, S. Wang, and R. Urtasun, "Deep continuous fusion for multi-sensor 3D object detection," in *ECCV*, 2018. DOI: [10.1007/978-3-030-01270-0\\_39](https://doi.org/10.1007/978-3-030-01270-0_39).
- [8] A. Geiger, P. Lenz, and R. Urtasun, "Are we ready for autonomous driving? the KITTI vision benchmark suite," in *CVPR*, 2012. DOI: [10.1109/CVPR.2012.6248074](https://doi.org/10.1109/CVPR.2012.6248074).
- [9] M. Cordts, M. Omran, S. Ramos, T. Rehfeld, M. Enzweiler, R. Benenson, U. Franke, S. Roth, and B. Schiele, "The cityscapes dataset for semantic urban scene understanding," in *CVPR*, 2016. DOI: [10.1109/CVPR.2016.350](https://doi.org/10.1109/CVPR.2016.350).
- [10] D. Bozhinoski, D. Di Ruscio, I. Malavolta, P. Pelliccione, and I. Crnkovic, "Safety for mobile robotic systems: A systematic mapping study from a software engineering perspective," *J. Syst. Softw.*, vol. 151, 2019. DOI: [10.1016/j.jss.2019.02.021](https://doi.org/10.1016/j.jss.2019.02.021).
- [11] V. S. Ramachandran and R. L. Gregory, "Perceptual filling in of artificially induced scotomas in human vision," *Nature*, vol. 350, no. 6320, 1991. DOI: [10.1038/350699a0](https://doi.org/10.1038/350699a0).
- [12] A. Malinin and M. Gales, "Predictive uncertainty estimation via prior networks," in *NEURIPS*, 2018.
- [13] N. Papernot and P. McDaniel, "Deep k-nearest neighbors: Towards confident, interpretable and robust deep learning," 2018. arXiv: [1803.04765 \[cs.LG\]](https://arxiv.org/abs/1803.04765).
- [14] D. Hendrycks and K. Gimpel, "A baseline for detecting misclassified and Out-of-Distribution examples in neural networks," in *ICLR*, 2017.
- [15] K. Lee, K. Lee, H. Lee, and J. Shin, "A simple unified framework for detecting Out-of-Distribution samples and adversarial attacks," in *NEURIPS*, 2018.
- [16] L. Ruff, R. Vandermeulen, N. Goernitz, L. Deecke, S. A. Siddiqui, A. Binder, E. Müller, and M. Kloft, "Deep one-class classification," in *ICML*, 2018.
- [17] I. Golan and R. El-Yaniv, "Deep anomaly detection using geometric transformations," in *NeurIPS*, 2018.
- [18] H. Choi, E. Jang, and A. A. Alemi, "WAIC, but why? Generative ensembles for robust anomaly detection," 2018. arXiv: [1810.01392 \[stat.ML\]](https://arxiv.org/abs/1810.01392).
- [19] M. Sabokrou, M. Khalooei, M. Fathy, and E. Adeli, "Adversarially learned one-class classifier for novelty detection," in *CVPR*, 2018. DOI: [10.1109/cvpr.2018.00356](https://doi.org/10.1109/cvpr.2018.00356).
- [20] S. Pidhorskyi, R. Almohsen, and G. Doretto, "Generative probabilistic novelty detection with adversarial autoencoders," in *NeurIPS*, 2018.
- [21] O. Ronneberger, P. Fischer, and T. Brox, "U-Net: Convolutional networks for biomedical image segmentation," in *Medical Image Computing and Computer-Assisted Intervention (MICCAI)*, 2015. DOI: [10.1007/978-3-319-24574-4\\_28](https://doi.org/10.1007/978-3-319-24574-4_28).
- [22] V. Badrinarayanan, A. Kendall, and R. Cipolla, "SegNet: A deep convolutional Encoder-Decoder architecture for image segmentation," *en, IEEE TPAMI*, vol. 39, no. 12, 2017. DOI: [10.1109/TPAMI.2016.2644615](https://doi.org/10.1109/TPAMI.2016.2644615).
- [23] L.-C. Chen, G. Papandreou, I. Kokkinos, K. Murphy, and A. L. Yuille, "DeepLab," *IEEE TPAMI*, 2016. DOI: [10.1109/TPAMI.2017.2699184](https://doi.org/10.1109/TPAMI.2017.2699184).
- [24] M. Everingham, L. Van Gool, C. K. I. Williams, J. Winn, and A. Zisserman, "The pascal visual object classes (VOC) challenge," *INTERNATIONAL JOURNAL OF COMPUTER VISION*, vol. 88, no. 2, 2010. DOI: [10.1007/s11263-009-0275-4](https://doi.org/10.1007/s11263-009-0275-4).
- [25] O. Zendel, K. Honauer, M. Murschitz, D. Steininger, and G. Fernandez Dominguez, "Wilddash-creating hazard-aware benchmarks," in *ECCV*, 2018. DOI: [10.1007/978-3-030-01231-1\\_25](https://doi.org/10.1007/978-3-030-01231-1_25).
- [26] G. Neuhold, T. Ollmann, S. R. Buló, and P. Kotschieder, "The mapillary vistas dataset for semantic understanding of street scenes," in *ICCV*, 2017. DOI: [10.1109/ICCV.2017.534](https://doi.org/10.1109/ICCV.2017.534).
- [27] C. Sakaridis, D. Dai, and L. Van Gool, "Semantic foggy scene understanding with synthetic data," *INTERNATIONAL JOURNAL OF COMPUTER VISION*, vol. 126, no. 9, 2018. DOI: [10.1007/s11263-018-1072-8](https://doi.org/10.1007/s11263-018-1072-8).
- [28] P. Bevandić, I. Krešo, M. Oršić, and S. Šegvić, "Discriminative out-of-distribution detection for semantic segmentation," 2018. arXiv: [1808.07703 \[cs.CV\]](https://arxiv.org/abs/1808.07703).
- [29] J. Mukhoti and Y. Gal, "Evaluating bayesian deep learning methods for semantic segmentation," 2018. arXiv: [1811.12709 \[cs.CV\]](https://arxiv.org/abs/1811.12709).

- [30] I. J. Goodfellow, J. Shlens, and C. Szegedy, “Explaining and harnessing adversarial examples,” in *ICLR*, 2015.
- [31] S. Liang, Y. Li, and R. Srikant, “Enhancing the reliability of out-of-distribution image detection in neural networks,” in *ICLR*, 2018.
- [32] C. Guo, G. Pleiss, Y. Sun, and K. Q. Weinberger, “On calibration of modern neural networks,” in *ICML*, 2017.
- [33] Y. Gal, “Uncertainty in deep learning,” PhD thesis, University of Cambridge, 2016.
- [34] A. Kendall and Y. Gal, “What uncertainties do we need in bayesian deep learning for computer vision?” In *NIPS*, 2017.
- [35] Y. Gal and Z. Ghahramani, “Dropout as a bayesian approximation: Representing model uncertainty in deep learning,” en, in *ICML*, 2016.
- [36] B. Lakshminarayanan, A. Pritzel, and C. Blundell, “Simple and scalable predictive uncertainty estimation using deep ensembles,” in *NIPS*, 2017.
- [37] K. Lee, H. Lee, K. Lee, and J. Shin, “Training confidence-calibrated classifiers for detecting Out-of-Distribution samples,” in *ICLR*, 2018.
- [38] A. Mandelbaum and D. Weinshall, “Distance-based confidence score for neural network classifiers,” 2017. arXiv: [1709.09844 \[cs.AI\]](#).
- [39] E. Nalisnick, A. Matsukawa, Y. W. Teh, D. Gorur, and B. Lakshminarayanan, “Do deep generative models know what they don’t know?” In *ICLR*, 2019.
- [40] C. Richter and N. Roy, “Safe visual navigation via deep learning and novelty detection,” in *Robotics: Science and Systems (RSS)*, 2017. DOI: [10.15607/RSS.2017.XIII.064](#).
- [41] C. Sakaridis, D. Dai, S. Hecker, and L. Van Gool, “Model adaptation with synthetic and real data for semantic dense foggy scene understanding,” in *ECCV*, 2018. DOI: [10.1007/978-3-030-01261-8\\_42](#).
- [42] D. Dai, C. Sakaridis, S. Hecker, and L. Van Gool, “Curriculum model adaptation with synthetic and real data for semantic foggy scene understanding,” 2019. arXiv: [1901.01415 \[cs.CV\]](#).
- [43] W. J. Youden, “Index for rating diagnostic tests,” en, *Cancer*, vol. 3, no. 1, 1950.
- [44] T. DeVries and G. W. Taylor, “Learning confidence for Out-of-Distribution detection in neural networks,” 2018. arXiv: [1802.04865 \[stat.ML\]](#).
- [45] L. Dinh, J. Sohl-Dickstein, and S. Bengio, “Density estimation using real NVP,” in *ICLR*, 2017.
- [46] D. P. Kingma and P. Dhariwal, “Glow: Generative flow with invertible 1x1 convolutions,” in *NEURIPS*, 2018.
- [47] L. Dinh, D. Krueger, and Y. Bengio, “NICE: Non-linear independent components estimation,” 2014. arXiv: [1410.8516 \[cs.LG\]](#).
- [48] J. V. Dillon, I. Langmore, D. Tran, E. Brevdo, S. Vasudevan, D. Moore, B. Patton, A. Alemi, M. Hoffman, and R. A. Saurous, “Tensorflow distributions,” 2017. arXiv: [1711.10604 \[cs.LG\]](#).
- [49] Y. A. Malkov and D. A. Yashunin, “Efficient and robust approximate nearest neighbor search using hierarchical navigable small world graphs,” 2016. arXiv: [1603.09320 \[cs.DS\]](#).
- [50] L. v. d. Maaten and G. Hinton, “Visualizing data using t-sne,” *Journal of Machine Learning Research*, vol. 9, no. Nov, 2008.

## Appendix

Here we provide details on the proposed datasets and the evaluated methods.

### A. Details on the Datasets

**FS OoD.** We apply the common evaluation mapping of the Cityscapes [9] classes using *road*, *sidewalk*, *building*, *wall*, *fence*, *pole*, *traffic light*, *traffic sign*, *vegetation*, *terrain*, *sky*, *person*, *rider*, *car*, *truck*, *bus*, *train*, *motorcycle*, *bicycle*. For OoD detection, the overlay object is labelled positive, any of the mentioned classes are negative, and void is ignored. Both the validation and the testset are created from the Cityscapes validation set, while they have strictly disjoint sets of overlay objects. The validation set was limited to 30 images to prevent few-shot learning and overfitting towards our method of sizing, placing and adjusting the overlay objects. While the absolute AP did not always match with the testset, we cross-checked that the relative ranking of methods was mostly preserved. In particular, we found results of parameter searches to be consistent between different random versions of the validation set. The complete validation set is part of the supplementary material.

**FS Misclassification.** From Foggy Driving [41], we select all images. From Foggy Zurich [42], we map classes *sky* and *fence* to *void*, as their labelling is not accurate and sometimes areas that are not visible due to fog are simply labelled *sky*. For WildDash [25], we use all images. For Mapillary Vistas [26], we sample 50 random images from the validation set and apply the label mapping described in Table 2.

During evaluation all pixels labelled as *void* are ignored.

### B. Details on the Methods

In this section we provide implementation details on the evaluated methods to ease the reproducibility of the results presented in this paper.

#### B.1. Semantic Segmentation Model

We use the state-of-the-art model DeepLabv3+ [1] with Xception-71 backbone, image-level features, and dense prediction cell. When no retraining is required, we use the original model trained on Cityscapes<sup>2</sup>.

#### B.2. Softmax

ODIN [31] applies input preprocessing and temperature scaling to improve the OoD detection ability of the maximum softmax probability. Early experiments on

<sup>2</sup><https://github.com/tensorflow/models/blob/master/research/deeplab>

| mapillary label                        | used label           |
|--|----------------------|
| <i>construction-barrier-fence</i>      | <i>fence</i>         |
| <i>construction-barrier-wall</i>       | <i>wall</i>          |
| <i>construction-flat-road</i>          | <i>road</i>          |
| <i>construction-flat-sidewalk</i>      | <i>sidewalk</i>      |
| <i>construction-structure-building</i> | <i>building</i>      |
| <i>human-person</i>                    | <i>person</i>        |
| <i>human-rider-*</i>                   | <i>rider</i>         |
| <i>nature-sky</i>                      | <i>sky</i>           |
| <i>nature-terrain</i>                  | <i>terrain</i>       |
| <i>nature-vegetation</i>               | <i>vegetation</i>    |
| <i>object-support-pole</i>             | <i>pole</i>          |
| <i>object-support-utility-pole</i>     | <i>pole</i>          |
| <i>object-traffic-light</i>            | <i>traffic light</i> |
| <i>object-traffic-sign-front</i>       | <i>traffic sign</i>  |
| <i>object-vehicle-bicycle</i>          | <i>bicycle</i>       |
| <i>object-vehicle-bus</i>              | <i>bus</i>           |
| <i>object-vehicle-car</i>              | <i>car</i>           |
| <i>object-vehicle-motorcycle</i>       | <i>motorcycle</i>    |
| <i>object-vehicle-on-rails</i>         | <i>train</i>         |
| <i>object-vehicle-truck</i>            | <i>truck</i>         |
| <i>marking-*</i>                       | <i>road</i>          |
| anything else                          | <i>void</i>          |

Table 2. Mapping of Mapillary classes onto our used set of classes for misclassification detection.

Fishyscapes showed that (i) temperature scaling did not improve much the results of this baseline, and (ii) input preprocessing w.r.t. the softmax score is not possible due to the limited GPU memory and the large size of the DeepLab model. As the maximum probability is anyway not competitive with respect to the other methods, we decided to not further develop that baseline.

#### B.3. Bayesian DeepLab

We reproduce the setup described by Mukhoti & Gal [29]. As such, we use the Xception-65 backbone pre-trained on ImageNet, and insert dropout layers in its middle flow. We train for 90k iterations, with a batch size of 16, a crop size of  $513 \times 513$ , and a learning rate of  $7 \cdot 10^{-3}$  with polynomial decay.

#### B.4. Dirichlet DeepLab

Following Malinin & Gales [12], we interpret the output logits of DeepLab as log-concentration parameters  $\alpha$

and train with the loss described by Equation (5) and implemented with the TensorFlow Probability [48] framework. For the first term, the target labels are smoothed with  $\epsilon = 0.01$  and scaled by  $\alpha_0 = 100$  to obtain target concentrations. To ensure convergence of the classifier, we found it necessary to downweight both the first and second terms by 0.1 and to initialize all but the last layer with the original DeepLab weights.

We also tried to replace the first term by the negative log-likelihood of the Dirichlet distribution but were unable to make the training converge.

### B.5. kNN Embedding

**Layer of Embedding.** As explained in Section 4.1, we had to restrict the kNN queries to one layer. A single layer of the network already has more than 10000 embedding vectors and we need to find  $k$  nearest neighbors for all of them. Querying over multiple layers therefore becomes infeasible. To select a layer of the network, we test multiple candidates on the FS OoD validation set. We experienced that our kNN fitting with *hnsplib*<sup>3</sup> [49] was not deterministic, therefore we provide the average performance on the validation set over 3 different experiments. Additionally, we had to reduce the complexity of kNN fitting by randomly sampling 1000 images from Cityscapes instead of the whole training set (2975 images).

For the kNN density, we provide the results for different layers in Table 3. We observe that the kNN embedding density is the only embedding based method that has a better AP in the decoder layers than in the xception layers.

| DeepLab Layer                         | AP         |
|---------------------------------------|------------|
| xception_71/middle_flow/block1/unit_8 | 15.2 ± .06 |
| xception_71/exit_flow/block2          | 17.6 ± .04 |
| aspp_features                         | 53.7 ± 1.4 |
| decoder_conv0_0                       | 43.7 ± 3.1 |
| decoder_conv1_0                       | 47.8 ± 3.7 |

Table 3. Parameter search of the **embedding layer for kNN density**. The AP is computed on the validation set of FS OoD. Based on these results, we use the layer `aspp_features` in all our experiments.

For class-based embedding, we perform a similar search for the choice of layer. The result can be found in Table 4.

**Number of Neighbors.** We select  $k$  according to Tables 5 and 6. All values are measured with the same kNN fitting. As the computational time for each query grows with  $k$ , small values are preferable. Note that by definition, the rel-

<sup>3</sup><https://github.com/nmslib/hnsplib>

| DeepLab Layer                          | AP        |
|--|-----------|
| xception_71/middle_flow/block1/unit_8  | 9.6 ± 0.0 |
| xception_71/middle_flow/block1/unit_10 | 9.7 ± 0.0 |
| xception_71/exit_flow/block2           | 9.7 ± 0.1 |
| aspp_features                          | 2.3 ± 0.7 |
| decoder_conv0_0                        | 2.8 ± 0.1 |
| decoder_conv1_0                        | 3.1 ± 0.2 |

Table 4. Parameter search of the **embedding layer for class based relative kNN density**. The AP is computed on the validation set of FS OoD. Based on these results, we use the layer `xception_71/exit_flow/block2` in all our experiments.

ative class density needs a sufficiently high  $k$  such that not all neighbors are from the same class.

| k   | AP   |
|-----|------|
| 1   | 42.3 |
| 2   | 44.6 |
| 5   | 47.7 |
| 10  | 50.9 |
| 20  | 52.2 |
| 50  | 52.7 |
| 100 | 52.5 |

Table 5. Parameter search for the **number of nearest neighbors for kNN embedding density**. As computing time increases with  $k$ , we select  $k = 20$ .

| k   | AP   |
|-----|------|
| 5   | 5.4  |
| 10  | 6.7  |
| 20  | 7.9  |
| 50  | 9.3  |
| 100 | 9.9  |
| 200 | 10.0 |

Table 6. Parameter search for the **number of nearest neighbors for the class based kNN relative density**. As computing time increases with  $k$ , we select  $k = 100$ .

### B.6. Learned Embedding Density

**Flow architecture.** The normalizing flow follows the simple architecture of Real-NVP. We stack 32 steps, each one composed of an affine coupling layer, a batch normalization

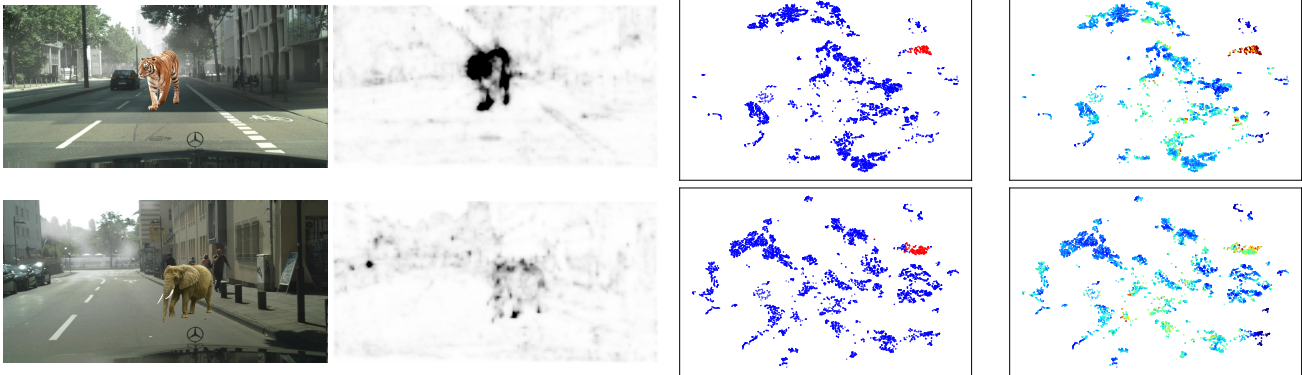


Figure 6. **Visualization of the embeddings of a DeepLab layer.** From left to right, we show (a) the input image, (b) the pixel-wise NLL predicted by the normalizing flow, (c) the embeddings colored in blue (red) when associated with ID (OoD) pixels, and (d) the embeddings colored by predicted NLL with the jet colormap (red means high NLL). The first row shows a successful OoD detection, and the second row a failure case.

layer, and a fixed random permutation. As recommended by [46], we initialize the weights of the coupling layers such that they initially perform identity transformations.

**Flow training.** For a given DeepLab layer, we export the embeddings computed on all the images of the Cityscapes training set. The number of such datapoints depends on the stride of the layer, and amounts to 22M for a stride of 16. We keep 2000 of them for validation and testing, and train on the remaining embeddings for 200k iterations, with a learning rate of  $10^{-4}$ , and the Adam optimizer. Note that we can compare flow models based on how well they fit the in-distribution embeddings, and thus do not require any OoD data for hyperparameter search.

**Layer selection.** OoD data is only required to select the layer at which the embeddings are extracted. The corresponding feature space should best separate OoD and ID data, such that OoD embeddings are assigned low likelihood. We found that it is critical to extract embeddings before ReLU activations, as some dimensions might be negative for all training points, thus making the training highly unstable. We show in Table 7 the AP on the Fishyscapes OoD validation set for different layers. We first observe that the best performing layers of the learned and kNN embedding densities are different. This might be explained by the fact that some layers, particularly the ones deeper into the network, as noted by [15], map ID images to simpler unimodal distributions that more easily approximated by the kNN kernel, while this does not matter much for a normalizing flow given the higher complexity that it can model. We also notice that overall layers in the encoder middle flow work best, while Mukhoti & Gal [29] insert dropout layers at this particular stage. While we do not know the reason behind this design decision, we hypothesize they found these layers to best model for the epistemic uncertainty.

| DeepLab layer                          | AP          |
|--|-------------|
| xception_71/entry_flow/block5          | 15.4        |
| xception_71/middle_flow/block1/unit_4  | 29.6        |
| xception_71/middle_flow/block1/unit_6  | <b>36.0</b> |
| xception_71/middle_flow/block1/unit_8  | 35.9        |
| xception_71/middle_flow/block1/unit_10 | 33.7        |
| xception_71/middle_flow/block1/unit_12 | 27.4        |
| aspp_features                          | -           |
| decoder_conv0_0                        | 01.0        |
| decoder_conv1_0                        | 26.8        |

Table 7. Cross-validation of the **embedding layer for the learned density.** The AP is computed on the validation set of FS OoD. Based on these results, we use the layer `xception_71/middle_flow/block1/unit_6` in all our experiments. We could not manage to make the training of the `aspp_features` layer converge, most likely due to a very peaky distribution that induces numerical instabilities.

**Effect of input preprocessing.** As previously reported by [15, 31], we observe that this simple input preprocessing brings substantial improvements to the detection score on the test set. We show in Table 8 the AP for different noise magnitudes  $\epsilon$ .

### C. Visualization of the Embeddings

We show in this section some visualizations of the embeddings, and the associated NLL predicted by the normalizing flow.

For some given examples, embeddings of the layer `xception_71/middle_flow/block1/unit_6` were computed and projected to a two-dimensional space using

| Noise $\epsilon$ | AP on FS OoD |             |
|------------------|--------------|-------------|
|                  | validation   | test        |
| None             | 36.0         | 52.5        |
| 0.1              | 38.4         | -           |
| 0.2              | 39.1         | -           |
| 0.25             | <b>39.2</b>  | <b>55.4</b> |
| 0.3              | <b>39.2</b>  | -           |
| 0.35             | <b>39.2</b>  | -           |
| 0.4              | 39.1         | -           |
| 0.5              | 39.0         | -           |
| 1.0              | 36.6         | -           |

Table 8. Cross-validation of the **input preprocessing for the learned density**. Based on these results, we apply noise with magnitude  $\epsilon = 0.25$  in all our experiments.

t-SNE [50]. We show the results in Figure 6. In case of a successful OoD detection, we observe that the OoD embeddings are well separated from the ID embeddings, and are consequently assigned a lower likelihood. In the case of a failure, the OoD embeddings are closer to the ID embeddings, and their predicted likelihood is closer to that of many ID embeddings. This however does not tell whether the failure is due to (i) the embedding function not being sufficiently discriminative, thus mapping some OoD and ID pixels to the same embeddings; or (ii) the density estimation flow not being flexible enough to assign a low likelihood to all areas not covered by ID examples.

As it is not trivial to perform such a visualization on the whole set of training embeddings, or to significantly improve the representation power of the normalizing flow, we leave a further investigation to future work.